JOURNAL OF SYNCHROTRON RADIATION

ISSN 1600-5775

Received 5 August 2020
Accepted 21 October 2020

Edited by G. Grübel, HASYLAB at DESY, Germany

Keywords: mid-infrared free-electron lasers; biological fossils; melanin; hydroxyapatite.

Supporting information: this article has supporting information at journals.iucr.org/s

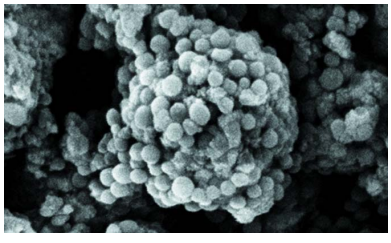

Application of mid-infrared free-electron laser for structural analysis of biological materials

Takayasu Kawasaki,[a]* Heishun Zen,[b] Kento Ozaki,[c] Hironari Yamada,[c] Kazumasa Wakamatsu[d] and Shosuke Ito[d]

[a]IR Free Electron Laser Research Center, Tokyo University of Science, 2641 Yamazaki, Noda, Chiba 278-8510, Japan, [b]Institute of Advanced Energy, Kyoto University, Gokasho, Uji, Kyoto 611-0011, Japan, [c]Photon Production Laboratory Ltd, 576-1 Anamura-cho, Kusatsu, Shiga 525-0012, Japan, and [d]Department of Chemistry, Fujita Health University School of Medical Sciences, 1-98 Dengakugakubo, Kutsukake-cho, Toyoake, Aichi 470-1192, Japan.
*Correspondence e-mail: kawasaki@rs.tus.ac.jp

A mid-infrared free-electron laser (MIR-FEL) is a synchrotron-radiation-based femto- to pico-second pulse laser. It has unique characteristics such as variable wavelengths in the infrared region and an intense pulse energy. So far, MIR-FELs have been utilized to perform multi-photon absorption reactions against various gas molecules and protein aggregates in physical chemistry and biomedical fields. However, the applicability of MIR-FELs for the structural analysis of solid materials is not well recognized in the analytical field. In the current study, an MIR-FEL is applied for the first time to analyse the internal structure of biological materials by using fossilized inks from cephalopods as the model sample. Two kinds of fossilized inks that were collected from different strata were irradiated at the dry state by tuning the oscillation wavelengths of the MIR-FEL to the phosphoryl stretching mode of hydroxyapatite (9.6 μm) and to the carbonyl stretching mode of melanin (5.8 μm), and the subsequent structural changes in those materials were observed by using infrared microscopy and far-infrared spectroscopy. The structural variation of these biological fossils is discussed based on the infrared-absorption spectral changes that were enhanced by the MIR-FEL irradiation, and the potential use of MIR-FELs for the structural evaluation of biomaterials is suggested.

1. Introduction

A free-electron laser (FEL) is an intense femto- to pico-second pulse laser generated by strong interaction of an accelerated electron beam with synchrotron radiation in a periodic magnetic field (O'Shea *et al.*, 2001). Basically, the oscillation wavelengths are ranged from X-ray to the far-infrared region, and X-ray FELs are well employed for analyses of structural dynamics of proteins and time-resolved analysis of enzymatic reactions in pharmaceutical and biochemical fields (Ishchenko *et al.*, 2019; Dasgupta *et al.*, 2019). Although these FEL operation systems have been developed at several traditional facilities such as CLIO, FELIX, J-Lab, ELBE and SACLA (Cohn *et al.*, 2015), the applicability of mid-infrared FELs (MIR-FELs) for the bio-related research fields is less recognized except for limited studies in pharmacy and surgical medicine (Auerhammer *et al.*, 1999; Fraschetti *et al.*, 2015; Kranenburg *et al.*, 2020; Sakamoto *et al.*, 2012; Edwards *et al.*, 2005; Mackanos *et al.*, 2005; Awazu *et al.*, 1998). A remarkable feature of MIR-FELs is that the oscillation wavelengths are tunable within the mid-infrared region from ∼3.5 to 25 μm, and there are many wavelengths resonant with various functional groups of biomolecules in

this fingerprint region (Bouchet *et al.*, 2017; Ziegler *et al.*, 2016). So far, this feature has enabled us to perform multi-photon absorption and excitation reactions against gas molecules in physical chemistry, biological pigments in dermatology and carbohydrate aggregates in environmental chemistry (Tono *et al.*, 2006; Kawasaki *et al.*, 2019, 2020*b*). For example, photodissociation spectroscopy analysis of ammonium cluster ions, photo-modification of aromatic compounds and cellulose degradation can be performed by using MIR-FELs. We also found that MIR-FELs can be effective for dissociation of protein aggregates that are associated with serious amyloidosis such as Alzheimer's disease (Kawasaki *et al.*, 2016, 2018). However, those studies were mainly aimed at removal of the pathogenic species from the normal tissues and structural remodelling of organic molecules by using an MIR-FEL as a laser scalpel, and the applicability of MIR-FELs for structural analysis of biomaterials is little known in the analytical field.

Here, we applied an MIR-FEL as a laser probe to explore the internal structure of biological materials for the first time. Melanin pigments are biological pigments ubiquitously present in bacteria, fungi, plants and animals (d'Ischia *et al.*, 2013). In the biosynthetic pathway of melanin, oxidation of tyrosine by tyrosinase leads to dark brown eumelanin polymers that consist of 5,6-dihydroxyindole (DHI) and 5,6-dihydroxyindole-2-carboxylic acid (DHICA) units, and the intervention of this process with cysteine results in the production of yellow to reddish brown pheomelanin. For the structural analysis of melanin, nuclear magnetic resonance (NMR), Fourier transform infrared (FT-IR) spectroscopy, electron paramagnetic resonance (EPR) and mass spectroscopy have been conventionally employed (Liu *et al.*, 2018; Prados-Rosales *et al.*, 2015; Xiao *et al.*, 2018). Alkaline hydrogen peroxide oxidation (AHPO), in particular, is a unique method to characterize eumelanin and pheomelanin (Ito *et al.*, 2011): pyrrole-2,3-dicarboxylic acid (PDCA), pyrrole-2,3,5-tricarboxylic acid (PTCA) and pyrrole-2,3,4,5-tetracarboxylic acid (PTeCA) can be produced by the AHPO treatment of DHI, DHICA and cross-linked DHI units of eumelanin, respectively (Ito *et al.*, 2013). In the course of our systematic study, two kinds of fossilized inks from cephalopods were identified: GSM122841 was collected from the Peterborough Member of the Oxford Clay Formation (Middle Jurassic, Late Callovian) at Christian Malford, Wiltshire, and YPM221210 was collected from the Koblenzer Bed of the Posidonia Shale Formation (Lower Jurassic, Early Toarcian, Tenuicostatum Zone) near Holzmaden, Baden-Württemberg (Glass *et al.*, 2012). Both fossils are composed of assemblies of many small particles where the diameter of each particle is ∼50–100 nm (Fig. 1). The dark pigments in the ink sacs were unambiguously identified as eumelanin by AHPO, EPR, solid state ^{13}C-NMR and FT-IR analyses, and other ingredients are hydroxyapatite, calcium carbonate and proteins in both fossilized inks, as estimated by elementary analysis (Barros *et al.*, 2019; Mürer *et al.*, 2018). However, it is yet unclear how eumelanin and these ingredients are intertwined to form a complex fossilized structure. Is the internal structure of GSM122841 different from that of YPM221210 or not?

In the current study, these biological fossils were irradiated using an MIR-FEL, and the subsequent structural changes were analysed by using mid-infrared microscopy and far-infrared spectroscopy.

2. Experimental

2.1. Materials

Fossilized ink sacs, GSM122841 and YPM221210, were obtained from Professor Derek E. G. Briggs (Yale University, New Haven, Connecticut, USA) and Dr Philip R. Wilby (British Geological Survey, Nottingham, UK), respectively. Detailed descriptions of these fossilized specimens can be found in previous articles (Glass *et al.*, 2013).

2.2. MIR-FEL instrument

We used the KU-FEL at the Institute of Advanced Energy, Kyoto University for the MIR-FEL irradiation experiments (Zen *et al.*, 2016). In brief, an electron beam that is generated by a high radio-frequency electron gun (2856 MHz) is accelerated by a linear accelerator and injected into a periodic magnetic field (undulator). The accelerated electron beam is forced to generate synchrotron radiation and the synchrotron radiation is amplified between the two resonant mirrors. The amplified synchrotron radiation can interact with the successive electron beam in the undulator and a part of the radiation beam can be extracted from a coupling hole in one mirror to produce an MIR-FEL. The MIR-FEL has a pulse train structure which consists of macro- and micro-pulses, where one macro-pulse oscillates at a repetition rate of 1.4 Hz and the typical pulse duration is 2 µs [see Fig. S1(*a*) in the supporting information]. One macro-pulse consists of several thousands of micro-pulses and the duration of each micro-

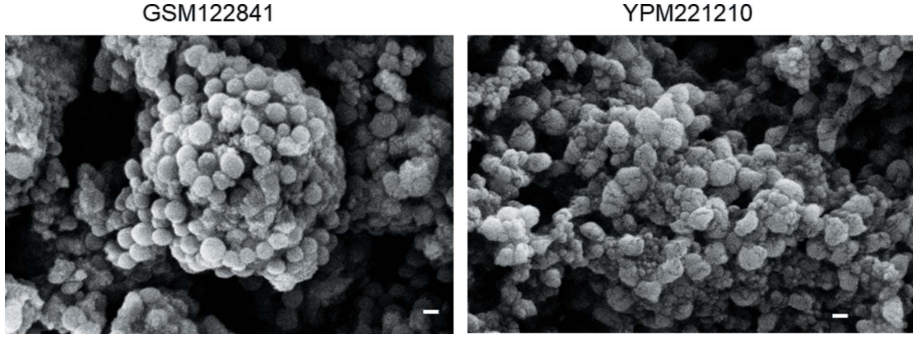

Figure 1
Scanning-electron-microscopy images of fossilized coleoid inks. GSM122841 (left) and YPM221210 (right). The bars represent 100 nm.

pulse is less than 1 ps. The oscillation wavelengths of the FEL are varied within the mid-infrared region (3.4–26 μm), and the half width of the diameter of the laser beam at the exit of the beamline was evaluated to be *ca.* 2 mm using the knife-edge method.

2.3. Laser irradiation

The powdered sample (*ca.* 5 mg) was irradiated with the MIR-FEL in a glass tube (1 cm in diameter and 3 cm in height) under atmosphere. The FEL beam was focused on the samples by using an off-axis parabola mirror, and the beam diameter above the surface of the sample was controlled to be less than 1 mm by changing the height of the sample stage. The laser power was tuned to 24–26 mJ per macro-pulse and the irradiation time was set to 10 min for all the samples and conditions. The glass tube was shaken horizontally to irradiate the whole surface of the powder uniformly. After irradiation, the powder was transferred to a stainless steel base by using water-dimethyl sulfoxide (DMSO) solution (500 μl) in a ratio of 9:1 and the dried film was directly inspected by optical and IR microscopies.

2.4. Optical microscopy

Fossils samples on the metal base were observed using an Area PIII-FX microscope (SK-Electronics Co. Ltd, Kyoto, Japan) with a high-magnification object lens (×200). A snapshot was obtained using a 12-million-pixel CCD camera under the halogen lamp. The image of the surface of the sample was analysed by *Perfect Viewer* 7 imaging software (SK-Electronics Co. Ltd, Kyoto, Japan).

2.5. Infrared microscopy (IRM)

The measurements of IR spectra for the fossilized samples were performed using an IRM-7000 coupled with an FT/IR-6100 spectrometer (Jasco Co.). The sample film on the metal base was observed using a 16× Cassegrain lens and IR spectra were recorded from 600 to 4000 cm^{-1} by 32 scans at 4 cm^{-1} resolution in reflection mode. The IR spectra were acquired by a lattice measurement: a total of ∼800 spectra were recorded with a 100 μm × 100 μm aperture from the sample surface (3 mm × 3 mm) and these spectra were used for mapping analysis by using *Spectra Manager* 2 software (Jasco Co.). In this imaging analysis, the *x*, *y* and *z* axes were set as follows: *x* and *y* are the horizontal and vertical lengths (μm) of the visual field on the sample, respectively, and *z* is the absorbance (in a.u.) of the mid-infrared spectrum of the sample.

2.6. Far-infrared spectroscopy

For the measurement of far-infrared spectra, an FT/IR-6200 spectrometer (Jasco Co.) was used. The sample was irradiated and dissolved in a water–DMSO solution, as mentioned in Section 2.3, and the solution (100 μl) was spread onto a polyethylene film with a diameter of 2 cm and a thickness of 1 mm. After drying, far-infrared spectra at 650–100 cm^{-1} were recorded by transmission mode with 64 scans.

3. Results

3.1. Effect of MIR-FEL irradiation targeting hydroxyapatite

In the mid-infrared absorption spectra of the two kinds of fossilized inks, three major bands were observed [Fig. 2(*a*)]: the highest peak at 1030–1040 cm^{-1} (∼9.5 μm) resonates with the phosphoryl stretching vibrational mode (νP═O) of hydroxyapatite, two peaks at 1425–1460 cm^{-1} correspond to $CaCO_3$, and the broad peak at 1600–1700 cm^{-1} (∼6 μm) resonates with carbonyl bonds (νC═O) in indole and pyrrole groups of melanin (Glass *et al.*, 2012). Hydroxyapatite and melanin are main components in these fossils and their IR absorption bands are independent of each IR spectrum. To reveal the structural features of the fossilized inks, hydroxyapatite and melanin were targeted by the MIR-FEL irradiation, and the laser wavelengths were tuned to 9.6 μm and

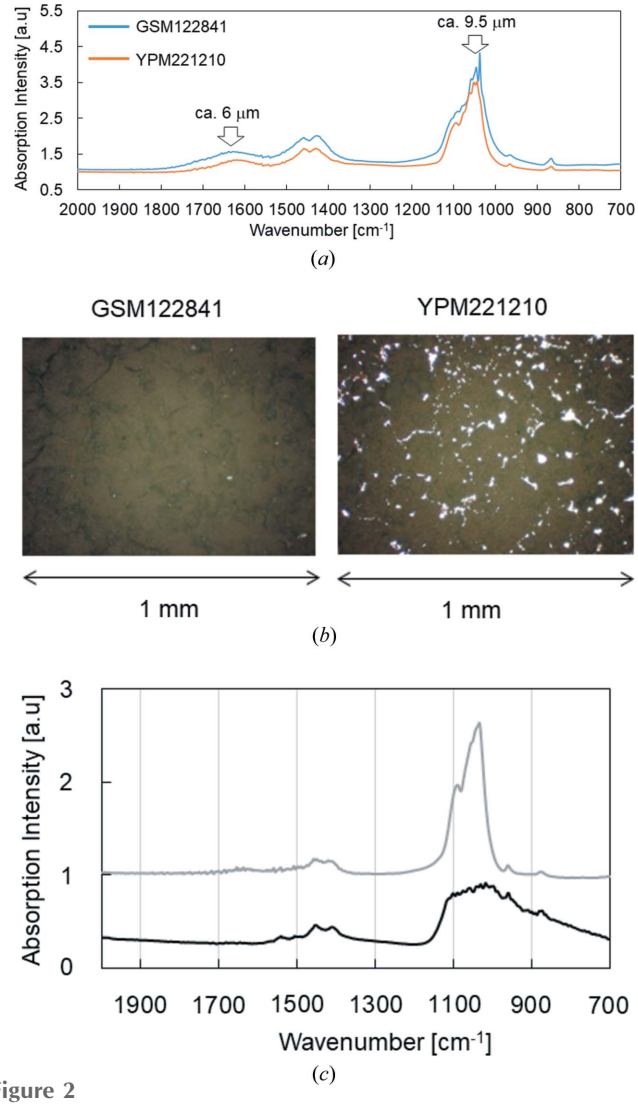

Figure 2
(*a*) Mid-infrared spectra of GSM122841 (blue curve) and YPM221210 (orange curve). Irradiation wavelengths of the MIR-FEL are indicated by arrows. (*b*) An optical microscope observation of fossilized coleoid inks on the slide base after irradiation tuned to 9.6 μm. (*c*) FT-IR spectra of hydroxyapatite before (grey) and after (black) the MIR-FEL irradiation at 9.6 μm.

5.8 µm, respectively [Figs. S1(*b*) and S1(*c*)]. Firstly, the effect of the irradiation targeting hydroxyapatite was tested. After the irradiation, the powder was suspended in aqueous solution, spread onto a metal base and dried under atmosphere [Fig. 2(*b*)] to analyse the sample surface by IRM.

The effect of MIR-FEL irradiation on hydroxyapatite alone and that on fossilized inks is shown in Figs. 2(*c*) and 3, respectively. It is evident that the strong P═O stretching vibrational peak at 1042 cm^{-1} is substantially decreased compared with the two small peaks at 1400–1500 cm^{-1} after the irradiation [Fig. 2(*c*)]. This decrease of the peak intensity indicates that the phosphoryl group in hydroxyapatite was decomposed by the irradiation. As shown in Fig. 3(*a*), almost all of the peak intensities at 1042 cm^{-1} on the surface of GSM122841 with the irradiation are quite lower compared with those without irradiation. In addition, the other absorption peaks shown in Figs. 3(*b*)–3(*d*) at 1425 cm^{-1}, 1460 cm^{-1} and 1626 cm^{-1} on the surface of GSM122841 are remarkably reduced by the irradiation compared with those without irradiation. These reductions in the mid-infrared absorption intensities indicate the substantial damage of the structure of GSM122841 caused by the MIR-FEL irradiation targeting hydroxyapatite. On the other hand, the peak distribution shown in Fig. 3(*a*) at 1042 cm^{-1} on the surface of the YPM221210 film is little changed, although other peak distributions shown in Figs. 3(*b*)–3(*d*) at 1425 cm^{-1}, 1460 cm^{-1} and 1626 cm^{-1} were somewhat altered by the irradiation. This indicates that YPM221210 was not considerably damaged by the irradiation targeting hydroxyapatite compared with GSM122841.

3.2. Effect of MIR-FEL irradiation targeting melanin

The melanin-targeted laser irradiation resulted in a significant reduction in peak intensities at 1626 cm^{-1} (νC═O) for both GSM122841 and YPM221210 [Fig. 4(*d*)]. On the other hand, the peak distribution at 1042 cm^{-1} is little changed in either sample [Fig. 4(*a*)]. These results indicate that the internal melanin was partly decomposed, although hydroxyapatite was hardly affected by the vibrational excitation of carbonyl bonds at 5.8 µm in both samples. Interestingly, peak distributions at 1425 cm^{-1} and 1460 cm^{-1} in GSM122841

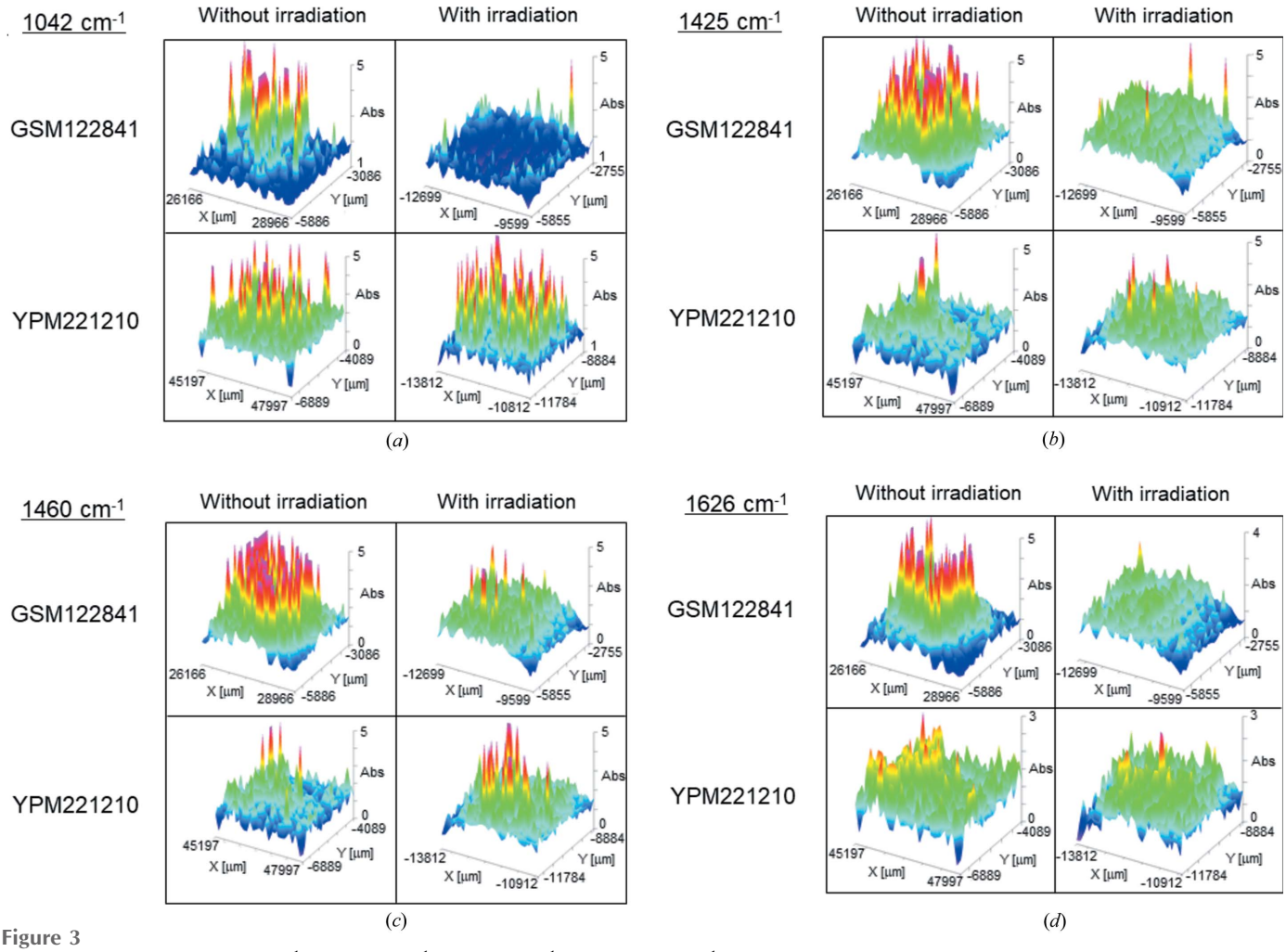

Figure 3
Peak distributions at (*a*) 1042 cm^{-1}, (*b*) 1425 cm^{-1}, (*c*) 1460 cm^{-1} and (*d*) 1626 cm^{-1}, with and without the MIR-FEL irradiation tuned to 9.6 µm on the surfaces of GSM122841 (upper) and YPM221210 (lower). Absorption intensities are categorized by four colours: blue (very weak), green (weak), yellow (strong) and red (very strong).

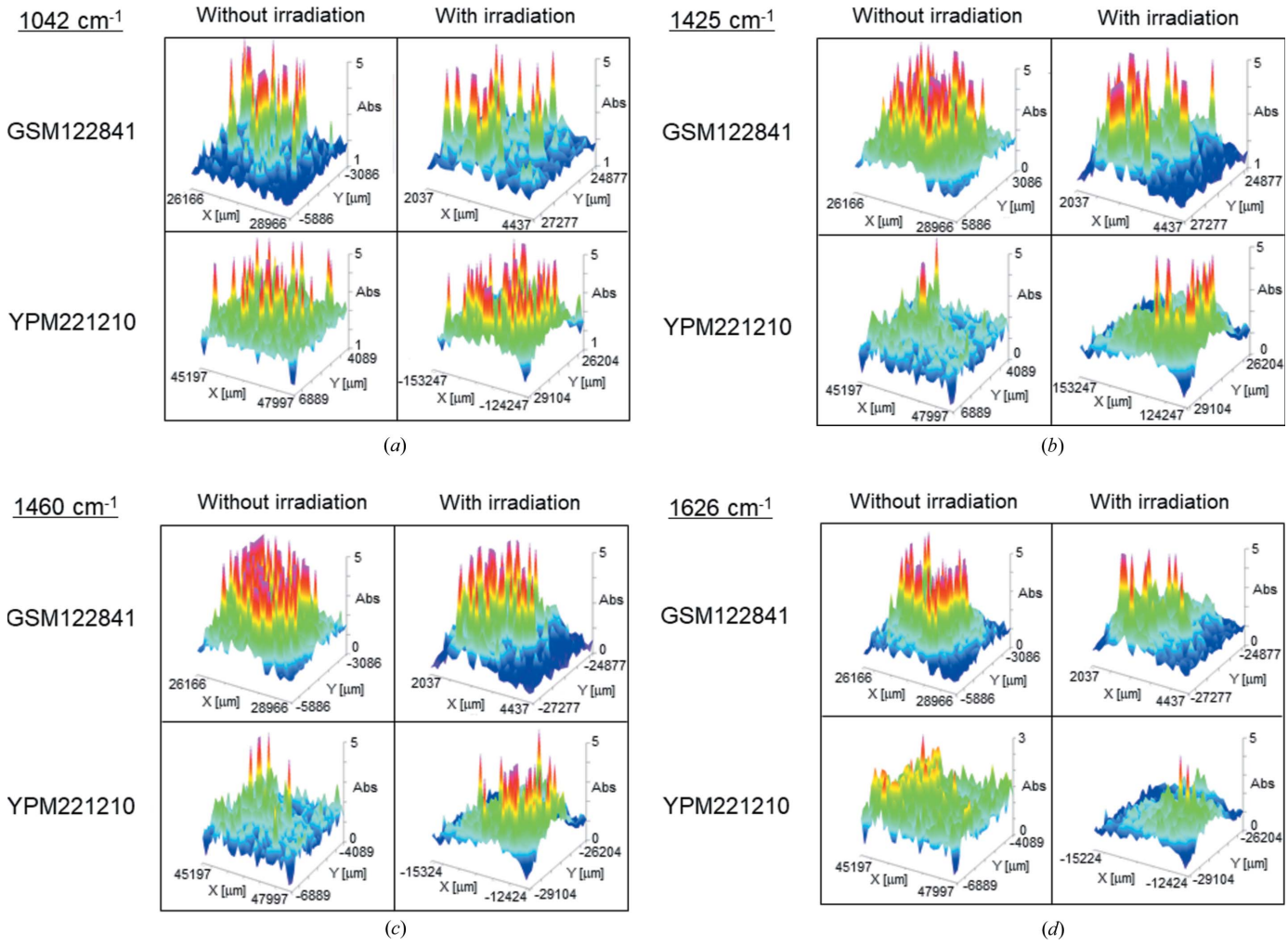

Figure 4
Peak distributions at (*a*) 1042 cm^{-1}, (*b*) 1425 cm^{-1}, (*c*) 1460 cm^{-1} and (*d*) 1626 cm^{-1}, with and without the MIR-FEL irradiation at 5.8 μm on the surfaces of GSM122841 (upper) and YPM221210 (lower). The colour categories are the same as Fig. 3.

[Figs. 4(*b*) and 4(*c*), upper] are little changed by the melanin-targeted irradiation, although they were mostly reduced by the hydroxyapatite-targeted irradiation [Figs. 3(*b*) and 3(*c*), upper]. This result indicates that the structure involving calcium carbonate in GSM122841 was little affected by the irradiation targeting melanin. On the contrary, those peak distributions in YPM221210 were somewhat modified by the irradiation targeting melanin [Figs. 4(*b*) and 4(*c*), lower], similarly with the case targeting hydroxyapatite [Figs. 3(*b*) and 3(*c*), lower].

To obtain more evidence for the structural difference between GSM122841 and YPM221210, we measured far-infrared spectra after the irradiation at 5.8 μm (Fig. 5). In both spectra before irradiation (solid line), broad bands from 100–400 cm^{-1} and two sharp peaks at 550–610 cm^{-1} were observed. Interestingly, spectral contour at 200–600 cm^{-1} is drastically changed and a strong peak at 475 cm^{-1} appears after the irradiation (dotted line) in the case of YPM221210 (right). On the contrary, such spectral change is not remarkable in the case of GSM122841 (left). In general, absorption intensity in the far-infrared region is influenced by the collective vibrational mode of the molecular assembly and tends to increase in the hydrated state

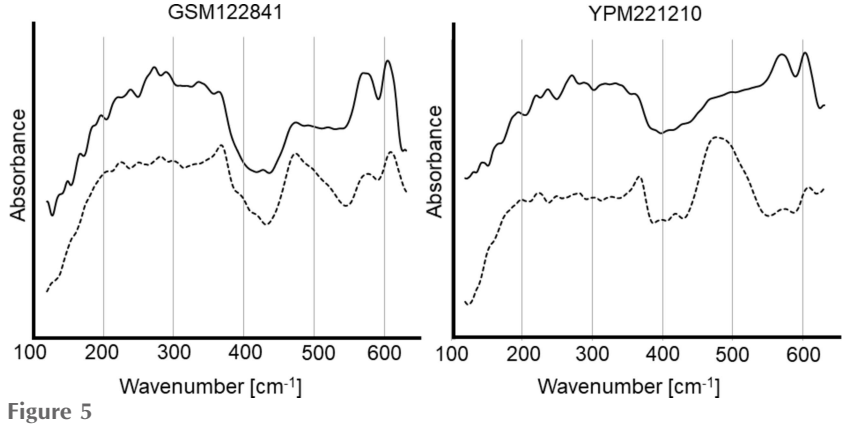

Figure 5
Far-infrared spectra of GSM122841 (left) and YPM221210 (right). The solid line represents the non-irradiated sample. The dotted line represents the sample after irradiation at 5.8 μm.

compared with that in the hydrophobic state (Png *et al.*, 2009; Niehues *et al.*, 2011). Biosynthesized melanin forms a hierarchical aggregate structure composed of intermolecular π-π stacked hydrophobic conformation of indole rings (Träg *et al.*, 2019; Ju *et al.*, 2018). Therefore, the large spectral change in the far-infrared region possibly indicates that the hydrophobic sheet conformation of YPM221210 was partially dissociated by the MIR-FEL irradiation targeting melanin, although the peak assignment at 475 cm^{-1} is not clear. The spectral changes in the mid-infrared region of YPM221210 [Figs. 4(*b*)–4(*d*)] may be a result of this conformational alteration of the molecular assembly of melanin.

4. Discussion

4.1. Insight into the structural variation of the fossilized inks

The above analytical results indicate a structural difference in the two kinds of fossilized coleoid inks: GSM122841 is decomposed by irradiation targeting hydroxyapatite and YPM221210 is little changed unless melanin is excited by irradiation. It can be suggested that the structure of GSM122841 is mainly occupied by hydroxyapatite compared with YPM221210, whereas YPM221210 is rigidly constructed by melanin involving calcium carbonate (Demény *et al.*, 2016). The structural toughness in the latter fossil may be caused by the complicated structure bridged with melanin. In a previous study, the degradation yields of PDCA, PTCA, and PTeCA from YPM221210 after AHPO treatment were remarkably lower than those from GSM122841, although atomic proportions of carbon, nitrogen, calcium and phosphorous in the former were higher compared with the latter (Glass *et al.*, 2013). This chemical analysis indicated that YPM221210 is structurally more rigid than GSM122841, and the current study using an MIR-FEL provides strong evidence for the structural difference relevant to the internal melanin between YPM221210 and GSM122841. In addition, we observed that a pyrrole group was decomposed when melanin powder was irradiated by an MIR-FEL at 5.8 µm (Kawasaki *et al.*, 2019). Based on this previous observation, it can be construed that the internal melanin in YPM221210 was similarly deformed by the IR radiation with the naked melanin, which caused obvious spectral changes in the mid- and far-infrared regions. The coleoid ink sacs produce and store a large amount of eumelanin that is used to avoid predation by enemies. Although fossilization of soft tissues such as ink sacs is rare, in fossil record, well preserved ink sacs have been discovered possibly because of the polymeric and highly cross-linked structure of eumelanin. According to the previous analysis using pyrolysis treatment (Glass *et al.*, 2013), it can be estimated that the structural feature of the fossilized inks may come from the preservation way of melanin and is generated by diagenesis processes, such as thermal maturation of geological formation. The variation of the structures of the fossilized inks may imply different diagenesis conditions in the ancient strata.

4.2. Applicability of MIR-FELs as the analytical tool for biomaterials

In the past, MIR-FELs were used for dissociation of protein aggregates such as amyloid fibrils (Kawasaki *et al.*, 2016, 2018, 2020*a*) and ablation of tissues in surgical medicine (Hutson *et al.*, 2009; Kanai *et al.*, 2008). However, we have shown another application example of MIR-FELs for exploring the structure of biological materials mediated by the mode-selective irradiation in the current study. It can be considered that the analytical approach using an MIR-FEL has the potential to become complementary to the conventional techniques such as NMR and FT-IR, and chemical techniques such as AHPO. For example, the structural composition of the targeted material can be estimated by measuring the IR spectral changes after the MIR-FEL irradiation tuned to specific wavelengths. In addition, some valuable information on the chemical structure of the ingredients can be gathered by the functional group selective vibrational excitation, if the detailed molecular structure of the target sample is unknown. The mid-infrared region contains 'fingerprinted' vibrational modes, and the MIR-FEL can give intense IR radiation energy to the individual functional group by state-selective excitation (Mankowsky *et al.*, 2014). Therefore, in principle, any biomaterials that can absorb the mid-infrared lights are potentially targeted by the MIR-FEL. Recently, high-throughput analysis has been required for rapid evaluation of structural substrates and organic polymer bases in pharmaceutical and material fields (Bader *et al.*, 2018; Rasi Ghaemi *et al.*, 2018). MIR-FELs are short-pulse lasers and the structural alteration in the targeted substance is triggered by the successive irradiation of micro-pulses within several microseconds. This short reaction time can allow us to evaluate many kinds of materials rapidly. Furthermore, IRM is a versatile analytical tool for investigating broad molecular compositions of biological tissues and biomaterials (Garidel *et al.*, 2007; Woess *et al.*, 2015; Stavitski *et al.*, 2013). The non-invasive and *in situ* convenient methods, in particular, are specific features of IRM for structural imaging of biological samples, and pathological and non-pathological species can be clearly discriminated on the vibrational signatures of the samples. Nowadays, synchrotron-radiation-based IRM beamlines can also be employed to improve the signal-to-noise ratio of the spectra of the observation targets. In the future, MIR-FELs can be expected to be used for structural estimation of not only biological samples but also solid functional materials by combination with IRM in various analytical fields. Nonetheless, samples are substantially damaged by the irradiation and are hardly recovered from the irradiated state. Therefore, abundant test samples should be applied to the structural analysis when using MIR-FELs.

5. Conclusions

Two kinds of fossilized coleoid inks, GSM122841 and YPM221210, were irradiated by a mid-infrared free-electron laser and analysed by infrared microscopy and far-infrared

spectroscopy. The irradiation at 9.6 μm that corresponded to the P═O stretch vibrational mode of hydroxyapatite induced remarkable decreases in peak intensities at the mid-infrared region in GSM122841, whereas little change was observed in YPM221210. The irradiation at 5.8 μm that resonated with the C═O stretch vibrational mode of melanin induced a significant decrease in peak intensity at 1626 cm^{-1} and drastic spectral change at ∼450 cm^{-1} in YPM221210 compared with GSM122841. These results indicate that YPM221210 is scarcely damaged by the MIR-FEL targeting hydroxyapatite, whereas it is rather labile when targeting melanin. In contrast, GSM122841 is easily broken by the irradiation targeting hydroxyapatite. This study for the first time shows that the composition of biomaterials can be evaluated by analysing the structural change induced by wavelength-specific infrared laser irradiation and opens a new avenue for the use of MIR-FELs in analytical and biomaterial fields.

Acknowledgements

This work was partly supported by the 'Joint Usage/Research Program on Zero-Emission Energy Research', Institute of Advanced Energy, Kyoto University (ZE30B-09). The authors thank Professor Derek E. G. Briggs (Yale University, New Haven, Connecticut, USA) and Dr Philip R. Wilby (British Geological Survey, Nottingham, UK) for supplying fossilized samples.

Funding information

This work was financially supported by Kao Melanin Workshop (grant number: A-1608).

References

Auerhammer, J. M., Walker, R., van der Meer, A. F. G. & Jean, B. (1999). *Appl. Phys. B*, **68**, 111–119.
Awazu, K., Nagai, A. & Aizawa, K. (1998). *Lasers Surg. Med.* **23**, 233–237.
Bader, A., Meiners, F. & Tracht, K. (2018). *Materials*, **11**, 1330.
Barros, O. A., Silva, J. H., Saraiva, G. D., Viana, B. C., Paschoal, A. R., Freire, P. T. C., Oliveira, N. C., Paula, A. J. & Viana, M. S. (2019). *PeerJ*, **7**, e6323.
Bouchet, A., Klyne, J., Ishiuchi, S. I., Fujii, M. & Dopfer, O. (2017). *Phys. Chem. Chem. Phys.* **19**, 10767–10776.
Cohn, K., Blau, J., Colson, W. B., Ng, J. & Price, M. (2015). *Proceedings of the 37th International Free Electron Laser Conference (FEL2015)*, 23–28 August 2015, Daejeon, Korea, pp. 625–629.
Dasgupta, M., Budday, D., de Oliveira, S. H. P., Madzelan, P., Marchany-Rivera, D., Seravalli, J., Hayes, B., Sierra, R. G., Boutet, S., Hunter, M. S., Alonso-Mori, R., Batyuk, A., Wierman, J., Lyubimov, A., Brewster, A. S., Sauter, N. K., Applegate, G. A., Tiwari, V. K., Berkowitz, D. B., Thompson, M. C., Cohen, A. E., Fraser, J. S., Wall, M. E., van den Bedem, H. & Wilson, M. A. (2019). *Proc. Natl Acad. Sci. USA*, **116**, 25634–25640.
Demény, A., Németh, P., Czuppon, G., Leél-Ossy, S., Szabó, M., Judik, K., Németh, T. & Stieber, J. (2016). *Sci. Rep.* **6**, 39602.
d'Ischia, M., Wakamatsu, K., Napolitano, A., Briganti, S., Garcia-Borron, J., Kovacs, D., Meredith, P., Pezzella, A., Picardo, M., Sarna, T., Simon, J. D. & Ito, S. (2013). *Pigm. Cell. Melanoma Res.* **26**, 616–633.
Edwards, G. S., Allen, S. J., Haglund, R. F., Nemanich, R. J., Redlich, B., Simon, J. D. & Yang, W. C. (2005). *Photochem. Photobiol.* **81**, 711–735.
Fraschetti, C., Filippi, A., Guarcini, L., Steinmetz, V. & Speranza, M. (2015). *J. Phys. Chem. B*, **119**, 6198–6203.
Garidel, P. & Boese, M. (2007). *Microsc. Res. Tech.* **70**, 336–349.
Glass, K., Ito, S., Wilby, P. R., Sota, T., Nakamura, A., Bowers, C. R., Vinther, J., Dutta, S., Summons, R., Briggs, D. E. G., Wakamatsu, K. & Simon, J. D. (2012). *Proc. Natl Acad. Sci. USA*, **109**, 10218–10223.
Glass, K., Ito, S., Wilby, P. R., Sota, T., Nakamura, A., Russell Bowers, C., Miller, K. E., Dutta, S., Summons, R. E., Briggs, D. E. G., Wakamatsu, K. & Simon, J. D. (2013). *Org. Geochem.* **64**, 29–37.
Hutson, M. S., Ivanov, B., Jayasinghe, A., Adunas, G., Xiao, Y., Guo, M. & Kozub, J. (2009). *Opt. Express*, **17**, 9840–9850.
Ishchenko, A., Stauch, B., Han, G. W., Batyuk, A., Shiriaeva, A., Li, C., Zatsepin, N., Weierstall, U., Liu, W., Nango, E., Nakane, T., Tanaka, R., Tono, K., Joti, Y., Iwata, S., Moraes, I., Gati, C. & Cherezov, V. (2019). *IUCrJ*, **6**, 1106–1119.
Ito, S., Nakanishi, Y., Valenzuela, R. K., Brilliant, M. H., Kolbe, L. & Wakamatsu, K. (2011). *Melanoma Res.* **24**, 605–613.
Ito, S., Wakamatsu, K., Glass, K. & Simon, J. D. (2013). *Anal. Biochem.* **434**, 221–225.
Ju, K. Y., Fischer, M. C. & Warren, W. S. (2018). *ACS Nano*, **12**, 12050–12061.
Kanai, T., Yoshihashi-Suzuki, S. & Awazu, K. (2008). *Appl. Opt.* **47**, 5862.
Kawasaki, T., Man, V. H., Sugimoto, Y., Sugiyama, N., Yamamoto, H., Tsukiyama, K., Wang, J., Derreumaux, P. & Nguyen, P. H. (2020*a*). *J. Phys. Chem. B*, **124**, 6266–6277.
Kawasaki, T., Sakai, T., Zen, H., Sumitomo, Y., Nogami, K., Hayakawa, K., Yaji, T., Ohta, T., Tsukiyama, K. & Hayakawa, Y. (2020*b*). *Energy Fuels*, **34**, 9064–9068.
Kawasaki, T., Sato, A., Tominaga, Y., Suzuki, Y., Oyama, T., Tadokoro, M., Tsukiyama, K., Nokihara, K. & Zen, H. (2019). *Photochem. Photobiol.* **95**, 946–950.
Kawasaki, T., Yaji, T., Ohta, T. & Tsukiyama, K. (2016). *J. Synchrotron Rad.* **23**, 152–157.
Kawasaki, T., Yaji, T., Ohta, T., Tsukiyama, K. & Nakamura, K. (2018). *Cell. Mol. Neurobiol.* **38**, 1039–1049.
Kranenburg, R. F., van Geenen, F. A. M. G., Berden, G., Oomens, J., Martens, J. & van Asten, A. C. (2020). *Anal. Chem.* **92**, 7282–7288.
Liu, Q., Xiao, J., Liu, B., Zhuang, Y. & Sun, L. (2018). *Int. J. Mol. Sci.* **19**, 3736.
Mackanos, M. A., Kozub, J. A. & Jansen, E. D. (2005). *Phys. Med. Biol.* **50**, 1871–1883.
Mankowsky, R., Subedi, A., Först, M., Mariager, S. O., Chollet, M., Lemke, H. T., Robinson, J. S., Glownia, J. M., Minitti, M. P., Frano, A., Fechner, M., Spaldin, N. A., Loew, T., Keimer, B., Georges, A. & Cavalleri, A. (2014). *Nature*, **516**, 71–73.
Mürer, F. K., Sanchez, S., Álvarez-Murga, M., Di Michiel, M., Pfeiffer, F., Bech, M. & Breiby, D. W. (2018). *Sci. Rep.* **8**, 10052.
Niehues, G., Heyden, M., Schmidt, D. A. & Havenith, M. (2011). *Faraday Discuss.* **150**, 193.
O'Shea, P. G. & Freund, H. P. (2001). *Science*, **292**, 1853–1858.
Png, G. M., Falconer, R. J., Fischer, B. M., Zakaria, H. A., Mickan, S. P., Middelberg, A. P. & Abbott, D. (2009). *Opt. Express*, **17**, 13102–13115.
Prados-Rosales, R., Toriola, S., Nakouzi, A., Chatterjee, S., Stark, R., Gerfen, G., Tumpowsky, P., Dadachova, E. & Casadevall, A. (2015). *J. Agric. Food Chem.* **63**, 7326–7332.
Rasi Ghaemi, S., Delalat, B., Gronthos, S., Alexander, M. R., Winkler, D. A., Hook, A. L. & Voelcker, N. H. (2018). *Appl. Mater. Interfaces*, **10**, 38739–38748.
Sakamoto, F. H., Doukas, A. G., Farinelli, W. A., Tannous, Z., Shinn, M., Benson, S., Williams, G. P., Gubeli, J. F. III, Dylla, H. F. & Anderson, R. R. (2012). *Lasers Surg. Med.* **44**, 175–183.

Stavitski, E., Smith, R. J., Bourassa, M. W., Acerbo, A. S., Carr, G. L. & Miller, L. M. (2013). *Anal. Chem.* **85**, 3599–3605.
Tono, K., Bito, K., Kondoh, H., Ohta, T. & Tsukiyama, K. (2006). *J. Chem. Phys.* **125**, 224305.
Träg, J., Duchstein, P., Hennemann, M., Clark, T., Guldi, D. M. & Zahn, D. (2019). *J. Phys. Chem. A*, **123**, 9403–9412.
Woess, C., Drach, M., Villunger, A., Tappert, R., Stalder, R. & Pallua, J. D. (2015). *Analyst*, **140**, 6363–6372.
Xiao, M., Chen, W., Li, W., Zhao, J., Hong, Y., Nishiyama, Y., Miyoshi, T., Shawkey, M. D. & Dhinojwala, A. (2018). *J. R. Soc. Interface.* **15**, 20180045.
Zen, H., Suphakul, S., Kii, T., Masuda, K. & Ohgaki, H. (2016). *Phys. Procedia*, **84**, 47–53.
Ziegler, B. E., Lecours, M., Marta, R. A., Featherstone, J., Fillion, E., Hopkins, W. S., Steinmetz, V., Keddie, N. S., O'Hagan, D. & McMahon, T. B. (2016). *J. Am. Chem. Soc.* **138**, 7460–7463.